Available online at www.sciencedirect.com
SCIENCE DIRECT®
Journal of Solid State Chemistry 178 (2005) 1254–1261
JOURNAL OF SOLID STATE CHEMISTRY
www.elsevier.com/locate/jssc

Synthesis of novel cation-ordered compounds with fluorite-related structure prepared by oxidation of Sn–Ta–O pyrochlore

Masao Kita[a], Takahisa Omata[a,*], Shinya Otsuka-Yao-Matsuo[a], Motomi Katada[b]

[a]*Department of Materials Science and Processing, Graduate School of Engineering, Osaka University, 2-1 Yamada-Oka, Suita-shi, Osaka-fu 565-0871, Japan*

[b]*Department of Chemistry, Graduate School of Science, Tokyo Metropolitan University, Minami-ohsawa, Hachioji 192-0397, Japan*

Received 30 September 2004; received in revised form 12 December 2004; accepted 28 January 2005

Abstract

Pyrochlore-type oxide, $Sn^{II}_{1.64}(Ta_{1.88}Sn^{IV}_{0.12})O_{6.58}$ was oxidized for exploring novel metastable phases. Two novel $Sn^{IV}_{0.82}(Ta_{0.94}Sn^{IV}_{0.06})O_{4.11}$ phases with a fluorite-related structure, which was obtained as a pure phase, and with a rutile-related structure appearing as an impurity for the fluorite-related phase were successfully obtained similar to the previous Sn–Nb–O system. The ordered arrangement of respective cations of Sn and (0.94Ta + 0.06Sn) in the precursor $Sn^{II}_{1.64}(Ta_{1.88}Sn^{IV}_{0.12})O_{6.58}$ was left in the both oxidized $Sn^{IV}_{0.82}(Ta_{0.94}Sn^{IV}_{0.06})O_{4.11}$ phases. In contrast to the previous Sn–Nb–O system, the cation-ordered α-PbO_2-related $Sn^{IV}_{0.82}(Ta_{0.94}Sn^{IV}_{0.06})O_{4.11}$ could not be obtained in the present conditions. Such a difference between the Sn–Ta–O and Sn–Nb–O systems was interpreted by larger energy barrier of the transformation from the fluorite-related phase to α-PbO_2-related phase in Sn–Ta–O system than in Sn–Nb–O system.

Keywords: Oxygen intercalation; Metastable phase; Cation-ordered structure; Pyrochlore structure; Fluorite structure; Phase transformation; Tin oxide; Tantalum oxide

1. Introduction

Since the discovery of the metastable cation-ordered fluorite-related $CeZrO_4$ phase [1], i.e., κ-$CeZrO_4$, which can be obtained by oxidation of $Ce_2Zr_2O_7$ pyrochlore at low temperature (approximately <1000 K), synthesis route of new metastable phases via pyrochlore-type precursor has attracted much interest in solid state chemistry [2–7]. The formation mechanism of the κ-$Ce^{IV}ZrO_4$ by oxidation of $Ce^{III}_2Zr_2O_7$ pyrochlore has been proposed as following [3]. The insertion of oxygen into the original quasi-oxygen site, 8*a*-site in space group *Fd3m*, in the $Ce^{III}_2Zr_2O_7$ pyrochlore and the oxidation from Ce^{III} to Ce^{IV} take place without cation diffusion because of the sufficiently low oxidizing temperatures. As a result, a fluorite-related framework and a respective ordered arrangement of Ce and Zr ions in the precursor pyrochlore is left in the oxidized κ-$CeZrO_4$ phase. The insertion of oxygen into $Ce^{III}_2Zr_2O_7$ lattice induces deviation of atomic positions of Ce, Zr and oxygen from those in the pyrochlore or the ideal fluorite structures [4,5]. Tolla and coworkers have reported the appearance of metastable $Ce^{IV}SnO_4$ ($Ce^{IV}_2Sn_2O_8$) phase by oxidation of $Ce^{III}_2Sn_2O_7$ pyrochlore [6]. The formation mechanism of the $Ce^{IV}SnO_4$ was similar to that of κ-$CeZrO_4$; both $Ce^{IV}SnO_4$ and κ-$CeZrO_4$ appeared by the insertion of oxygen into the quasi-oxygen site in the precursor pyrochlore phases accompanying the oxidation from Ce^{III} to Ce^{IV}. Such a formation process of the metastable phases should be applicable for the other systems, in which a pyrochlore-type phase containing cations at the lower valence state such as Ce^{III} exists.

Recently, we have reported the formation of metastable phases in Sn–Nb–O system [8,9]. In that case, the

*Corresponding author. Fax: +81 6879 7464.
E-mail address: omata@mat.eng.osaka-u.ac.jp (T. Omata).

0022-4596/$ - see front matter © 2005 Elsevier Inc. All rights reserved.
doi:10.1016/j.jssc.2005.01.029

pyrochlore phase with a composition of $Sn^{II}_{1.62}(Nb_{1.86}Sn^{IV}_{0.14})O_{6.55}$ was applied as a precursor phase. Novel metastable $Sn^{IV}_{0.81}(Nb_{0.93}Sn^{IV}_{0.07})O_{4.085}$ phases have been successfully synthesized by oxidation of the precursor $Sn^{II}_{1.62}(Nb_{1.86}Sn^{IV}_{0.14})O_{6.55}$. By changing the oxidation condition of the precursor, i.e., temperature and the oxygen partial pressure, three kinds of $Sn^{IV}_{0.81}(Nb_{0.93}Sn^{IV}_{0.07})O_{4.085}$ phases were formed. One was the cation-ordered fluorite-related phase like the κ-$CeZrO_4$. The other two novel phases were α-PbO_2 and rutile-related phases. The formation mechanism of α-PbO_2 and rutile-related phases were explained by the sliding of oxygen stacking in the transiently formed cation-ordered fluorite-related phase; such a transformation among the fluorite, rutile and α-PbO_2 structures is well-known as a phenomenon under high pressure over 10 GPa [10–13]. Because the sliding of oxygen stacking occurs without cation diffusion, the respective ordered arrangement of Sn and (0.93Nb + 0.07Sn) in the precursor pyrochlore was left in the resulting α-PbO_2 and rutile-related phases. The synthesis route applying such a transformation from the fluorite-related phase into α-PbO_2 or rutile-related phases are expected as a new route to explore novel metastable phases.

It is known that the pyrochlore phase containing Sn^{II} ion appears in the Sn–Ta–O system [14,15]. In the present study, we have attempted to synthesis new metastable phases in Sn–Ta–O system by oxidation of the pyrochlore phase. On the basis of the previous experiments in Sn–Nb–O system, the oxygen partial pressure and the temperature during the oxidation were controlled as synthesis valuables. The precursor and its oxidized phases were identified by powder X-ray diffraction (XRD) technique. Chemical compositions were evaluated from the atomic ratio of cations obtained by inductively coupled plasma (ICP) spectroscopy and oxygen concentration obtained by thermogravimetry (TG). The valence state of tin was also studied by ^{119}Sn Mössbauer spectroscopy.

2. Experimental

2.1. Preparation of the precursor $Sn^{II}_{1.64}(Ta_{1.88}Sn^{IV}_{0.12})O_{6.58}$ pyrochlore

The pyrochlore-type precursor in Sn–Ta–O system was prepared as follows. Powdered raw materials SnO (3 N) and Ta_2O_5 (3 N) were thoroughly mixed in a molar ratio of 2:1 using a zirconia mortar, and pressed into 9-mm-diameter disks under 100 MPa. The disks were placed in a silica glass ampoule (17-mm i.d.); the ampoule was evacuated to under 1×10^{-4} Pa using an oil diffusion pump, and then sealed. After the disks in the ampoule were fired at 1173 K for 5 h, they were cooled to a room temperature in the furnace. The as-sintered samples contained very small amount of metallic tin in addition to the pyrochlore-type phase. After the sample was washed in 0.1 N HNO_3 aq. to eliminate the impurity metallic tin, it was supplied as a precursor Sn–Ta–O pyrochlore phase. The Sn–Ta–O pyrochlore obtained was supplied to TG and differential thermal analysis (DTA) (Seiko Instruments TG/DTA320) up to 1573 K under O_2 gas flow in order to evaluate the oxygen concentration in the phase. The atomic ratio of Sn and Ta for the precursor Sn–Ta–O pyrochlore was determined by the ICP emission spectroscopy. The composition and the cation distributions of the precursor pyrochlore phase were studied by the Rietveld analysis of its XRD profile. The sample was prepared carefully without rubbing in order to have less preferred orientation. The Rietveld analysis was carried out in the 2θ range of 10–80° using the code Rietan 2000 written by Izumi [16].

2.2. Oxidation of the precursor $Sn^{II}_{1.64}(Ta_{1.88}Sn^{IV}_{0.12})O_{6.58}$ pyrochlore

The precursor Sn–Ta–O pyrochlore was oxidized in a flow of 1% O_2/Ar or O_2 gas in the following procedures. The powdered precursor of approximately 0.3 g loaded in an alumina crucible was set in the closed-end-type silica glass tube (19-mm i.d.). Then the tube was placed in a furnace and connected to an evacuation system with a rotary vacuum pump and a gas flow system. In order to avoid the oxidation of the precursor in the heating process, the silica glass tube was kept evacuated during the heating. After a pre-selected oxidation temperature of 573–973 K was attained, the evacuation was stopped and the oxidizing gas of 1% O_2/Ar or O_2 was introduced with a flow rate of 100 ml min^{-1}. After the oxidation for 5 h, the silica glass tube was removed from the furnace and cooled to room temperature; the oxidizing gas was kept flowing during the cooling process.

The crystalline phases obtained were identified by the XRD method. Lattice parameters of the oxidized phases were calculated using the least-square procedure. High-purity silicon powder (5 N) was mixed with the sample as an internal standard. The atomic ratio of Sn and Ta for the oxidized phase was determined by the ICP emission spectroscopy.

2.3. ^{119}Sn Mössbauer spectroscopy

The ^{119}Sn Mössbauer spectra of the precursor and its oxidized phases were recorded in the constant acceleration mode by transmission on a conventional spectrometer at room temperature. The source used was $Ca^{119m}SnO_3$ (185 MBq). Calibration of the velocity scale was made by using iron metal as a standard absorber, using ^{57}Co(Rh) as a source. The origin of the isomer

shift was determined from the center of the $BaSnO_3$ spectrum.

3. Results

3.1. Precursor $Sn^{II}_{1.64}(Ta_{1.88}Sn^{IV}_{0.12})O_{6.58}$ phase

Fig. 1 (a) shows the powder XRD profile of the precursor obtained. All the diffractions observed were indexed as those of cubic pyrochlore structure with the space group *Fd3m* (No. 227). The precursor prepared was identified as a single phase with a pyrochlore structure, because no diffraction due to impurity phase was observed. The lattice parameter for the Sn–Ta–O pyrochlore phase was calculated as $a = 1.05675(2)$ nm.

Fig. 2 shows the results of TG–DTA analysis under O_2 flow for the precursor pyrochlore as a starting sample. The TG curve showed an abrupt mass increase between 657 and 787 K, and showed constant mass above 873 K; the mass increase gently started above 373 K. The total mass increase was 1.305 mg for 32.610 mg of the starting pyrochlore. In the DTA curve, a clear exothermal peak corresponding to the mass

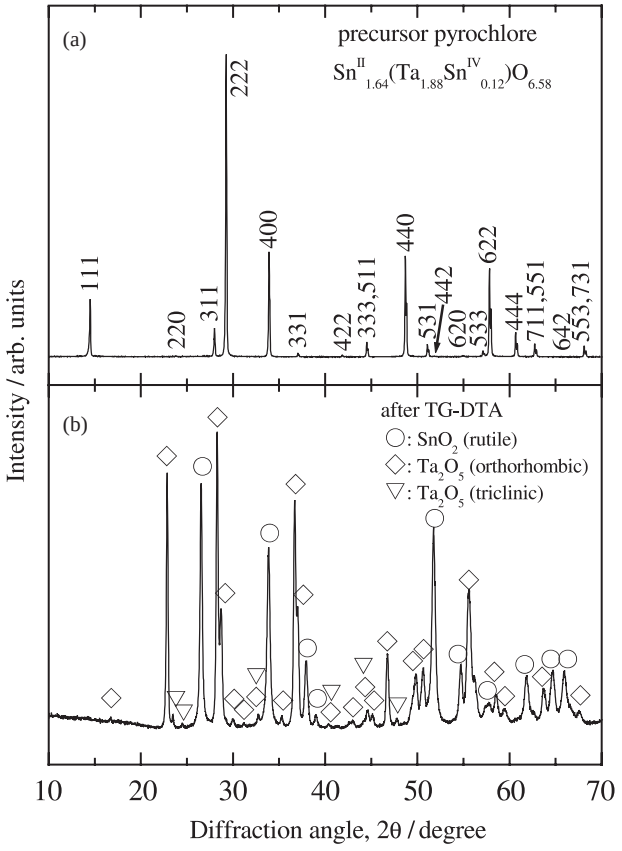

Fig. 1. Powder XRD patterns of (a) the precursor Sn–Ta–O pyrochlore, $Sn^{II}_{1.64}(Ta_{1.88}Sn^{IV}_{0.12})O_{6.58}$, and (b) the sample after TG–DTA analysis, in which the precursor pyrochlore was used as a starting material, up to 1573 K.

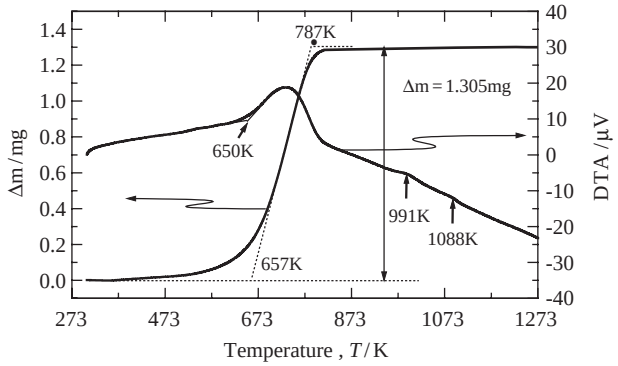

Fig. 2. TG and DTA curves for the precursor Sn–Ta–O pyrochlore, $Sn^{II}_{1.64}(Ta_{1.88}Sn^{IV}_{0.12})O_{6.58}$. The TG–DTA analysis was carried out under O_2 flow (100 ml min^{-1}) and a heating rate of 10 K min^{-1}.

increase was started at 650 K; two small bumps, which accompanied no mass change, were observed around 991 and 1088 K. After the analysis up to 1573 K, the sample became a mixture of SnO_2 and Ta_2O_5 phases as shown in Fig. 1(b). Therefore, the observed mass increase was attributed to the oxidation of divalent Sn^{II} in the precursor pyrochlore to tetravalent Sn^{IV} in the resulting SnO_2. The DTA peaks around 991 and 1088 K should be attributable to the decomposition into SnO_2 and Ta_2O_5. Fig. 3(a) shows ^{119}Sn Mössbauer spectrum of the precursor pyrochlore phase. The Mössbauer parameters obtained are summarized in Table 1. A singlet at 0.14 mm s^{-1} attributable to Sn^{IV} and two doublet centered at 3.26 and 3.57 mm s^{-1} attributable to Sn^{II} were observed in the spectrum. The spectrum agreed well with that previously reported for Sn–Nb–O pyrochlore [8,9,14,17]. The Mössbauer results showed that the precursor pyrochlore contained divalent Sn^{II} and tetravalent Sn^{IV}. Therefore, the composition of the precursor could be expressed as $Sn^{II}_x(Ta_{2-y}Sn^{IV}_y)O_{(x-0.5y+5)}$, assuming that the 16*c*-site of the pyrochlore was fully occupied by Ta and Sn^{IV} ions similar to the Sn–Nb–O pyrochlore [18]. After the TG analysis, the $Sn^{II}_x(Ta_{2-y}Sn^{IV}_y)O_{(x-0.5y+5)}$ pyrochlore was oxidized and decomposed into $(x+y)Sn^{IV}O_2$ and $(1-0.5y)Ta_2O_5$; for instance the number of oxygen atoms in mol of precursor increased from $(x-0.5y+5)$ to $(2x-0.5y+5)$ by oxidation of divalent Sn^{II} to tetravalent Sn^{IV}, i.e., increase in oxygen in mol agrees the Sn^{II} content, x. The mass increase obtained by TG analysis corresponded to the increase in the number of oxygen atoms of x. According to ICP analysis, the atomic ratio of Sn and Ta in the precursor pyrochlore was $X_{Sn} : X_{Ta} = (x+y) : (2-y) = 0.9345 : 1$ in mol. From these conditions, the composition of precursor pyrochlore was calculated as $Sn^{II}_{1.64}(Ta_{1.88}Sn^{IV}_{0.12})O_{6.58}$.

The composition and the cation distribution of the precursor $Sn^{II}_{1.64}(Ta_{1.88}Sn^{IV}_{0.12})O_{6.58}$ were also studied by Rietveld analysis, using the atomic parameters for

$Sn^{II}_{1.43}(Nb_{1.84}Sn^{IV}_{0.16})O_{6.35}$ pyrochlore reported by Cruz et al. [18] as initial values. The site occupancies were based on the chemical composition above described and fixed. The resulting profile is displayed in Fig. 4. The calculated profile of the pyrochlore with the space group *Fd3m* (No. 227) showed a good agreement with the observed data. Therefore, it was confirmed that the chemical formula $Sn^{II}_{1.64}(Ta_{1.88}Sn^{IV}_{0.12})O_{6.58}$ reasonably expressed the composition and the cation distribution of the precursor pyrochlore phase. The final atomic parameters and the inter-atomic distances are respectively summarized in Tables 2 and 3. Based on these chemical and structural analyses, it should be noted that the $Sn^{II}_{1.64}(Ta_{1.88}Sn^{IV}_{0.12})O_{6.58}$ pyrochlore possessed similar characteristics to that of $Sn^{II}_{1.43}(Nb_{1.84}Sn^{IV}_{0.16})O_{6.35}$ pyrochlore [18] as follows: (i) Sn^{II} is partially oxidized to Sn^{IV} and the Sn^{IV} occupies a part of Ta-site (16*c*-site), (ii) Sn^{II} occupied 96*g*- and 96*h*-sites, which correspond to the 16*d*-site in the ideal pyrochlore structure, (iii) Sn^{II} was partially deficient and (iv) the partial deficiency of Sn^{II} was electrically compensated by oxygen deficiency at 8*b*-site.

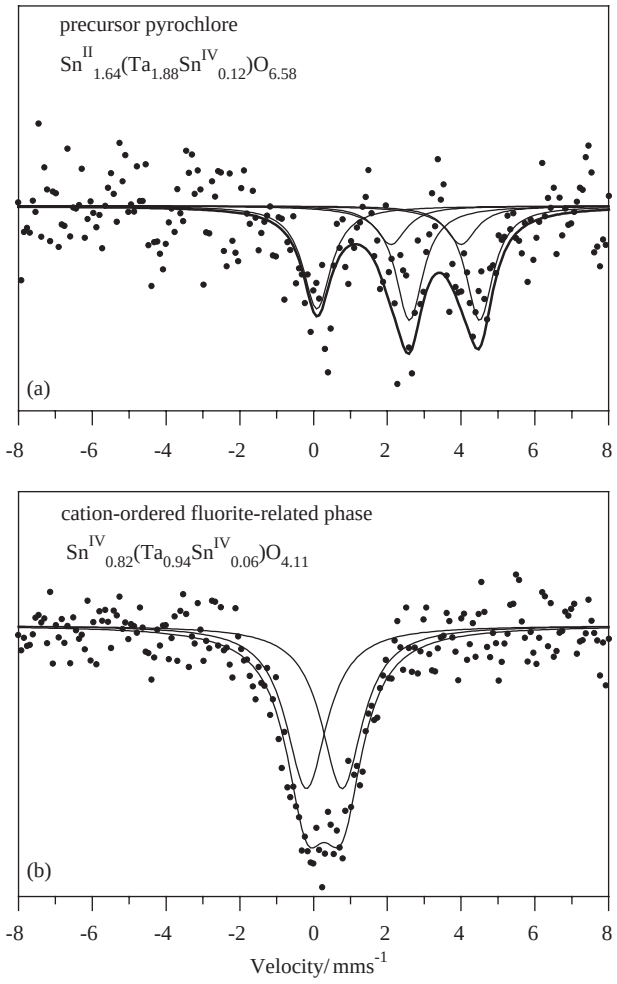

Fig. 3. ^{119}Sn Mössbauer spectra of (a) the precursor pyrochlore and (b) its oxidized phase at 673 K for 5 h in O_2.

3.2. Oxidation of the precursor

Fig. 5 shows the powder XRD patterns of the samples obtained by the precursor oxidation at 573–973 K for 5 h under O_2 gas flow. When the precursor was oxidized at 573 K, broad shoulder around 30° appeared; the diffraction angle of the shoulder was distinctly isolated from the diffraction of the precursor. For the oxidation at 673 K, the diffractions due to the precursor pyrochlore phase completely vanished, and the diffraction peaks indicated by the symbol ○ were observed. The diffraction profile for the sample oxidized at 673 K was very similar to that for the precursor pyrochlore, however, the diffraction angles were clearly higher than

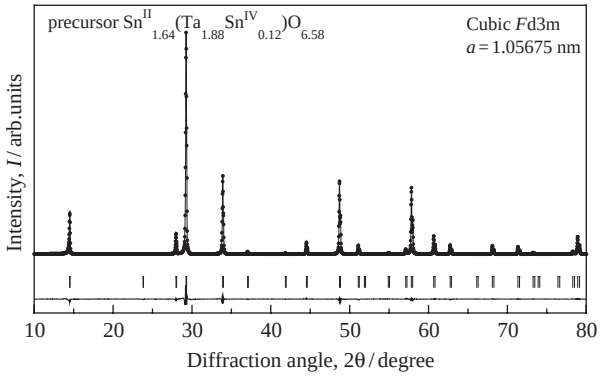

Fig. 4. Rietveld refinement profiles for the precursor $Sn^{II}_{1.64}(Ta_{1.88}Sn^{IV}_{0.12})O_{6.58}$ pyrochlore with the space group *Fd3m* (No. 227). The observed data are shown as dots, the calculated profile is the solid line and the difference curve between observed and calculated intensity is shown at the bottom of the figure. Tick marks represent the positions of possible Bragg reflections.

Table 1
Mössbauer parameters for the precursor pyrochlore and its oxidized phases

Sample	Isomer shift (*IS*) ($mm\,s^{-1}$)	Quadrupole splitting (*QS*) ($mm\,s^{-1}$)	FWHM (*Γ*) ($mm\,s^{-1}$)
Precursor pyrochlore $Sn^{II}_{1.64}(Ta_{1.88}Sn^{IV}_{0.12})O_{6.58}$	3.26	1.82	0.68
	3.57	1.91	0.72
	0.14	—	1.13
Cation-ordered fluorite-related $Sn^{IV}_{0.82}(Ta_{0.94}Sn^{IV}_{0.06})O_{4.11}$	0.25	0.97	1.29

Table 2
Results of the Rietveld refinement of the precursor $Sn^{II}_{1.64}(Ta_{1.88}Sn^{IV}_{0.12})O_{6.58}$ in the space group *Fd3m* (No. 227)

Atom	Site	*x*	*y*	*z*	Occupancy	B_{iso} (nm^2)
Ta	16*c*	0	0	0	0.94	0.0069(2)
Sn^{IV}	16*c*	0	0	0	0.06	0.0069(2)
Sn^{II} 1	96*g*	0.4819(8)	0.4819(8)	0.521(1)	0.0683[a]	0.0191(4)
Sn^{II} 2	96*h*	0	0.2748(2)	−0.2748(2)	0.0683[a]	0.0191(4)
O1	48*f*	0.3082(4)	1/8	1/8	1	0.017(1)
O2	8*b*	3/8	3/8	3/8	0.58	0.017(1)

Note: Lattice parameter $a = 1.05675$ nm. *R* factors (%): $R_{wp} = 7.47$, $R_p = 5.48$, $\chi^2 = 2.5778$ (refinement program: Rietan2000).
[a]Parameters constrained to be equal.

those for the precursor. Consequently, the sample obtained at 673 K was identified as novel cation-ordered fluorite-related Sn^{IV}–Ta–O phase. For the oxidation at 773 and 973 K, decomposition into SnO_2 and Ta_2O_5 occurred.

Fig. 6 shows the powder XRD patterns of the samples obtained by oxidation at 573–973 K for 5 h under 1% O_2/Ar gas flow. For the oxidation at 673 K, the precursor pyrochlore completely transformed into the same phase as observed in Fig. 5, i.e., cation-ordered fluorite-related phase. Above 773 K, small diffractions indicated by □ additionally appeared; their intensities slightly increased with increasing oxidation temperature. The diffractions indicated by □ were identified as those of rutile-related phase. According to the transformation mechanism previously proposed for Sn–Nb–O system [8], it is inferred that respective ordered arrangement of cations in the precursor pyrochlore is left in the rutile-related phase. In the previous Sn–Nb–O system, the oxidation under O_2 atmosphere transformed the precursor pyrochlore into cation-ordered α-PbO_2-related phase. The cation-ordered fluorite and rutile-related phases appeared by the oxidation under 1% O_2/Ar atmosphere. In contrast to the Sn–Nb–O system, under both atmospheres of 1% O_2/Ar and O_2, cation-ordered α-PbO_2-related phase did not appear.

The ^{119}Sn Mössbauer spectrum of the cation-ordered fluorite-related phase, which was obtained by the oxidation of the precursor at 673 K for 5 h under O_2 flow, is shown in Fig. 3(b). A quadrupole splitting doublet at *I.S.*∼0 was observed. The *I.S.* value showed that all Sn ions in the oxidized phases were tetravalent Sn^{IV}, and divalent Sn^{II} did not exist. The atomic ratio between Sn and Ta in the oxidized phases obtained from ICP analysis was the same as that in the precursor. The composition of the precursor was $Sn^{II}_{1.64}(Ta_{1.88}Sn^{IV}_{0.12})O_{6.58}$, thus, the composition for the oxidized phase was evaluated as $Sn^{IV}_{0.82}(Ta_{0.94}Sn^{IV}_{0.06})O_{4.11}$ [$Sn^{IV}_{1.64}(Ta_{1.88}Sn^{IV}_{0.12})O_{8.22}$]. Taking into consideration the practically low oxidation temperature of 673 K, it is not reasonable that the cations in the precursor phase diffuse during the oxidation. Thus, we concluded that respective ordered arrangement of Sn and (0.94Ta + 0.06Sn) in the precursor should be left in the oxidized $Sn^{IV}_{0.82}(Ta_{0.94}Sn^{IV}_{0.06})O_{4.11}$.

4. Discussion

Two novel metastable $Sn^{IV}_{0.82}(Ta_{0.94}Sn^{IV}_{0.06})O_{4.11}$ phases, in which the cations of Sn and (0.94Ta+0.06Sn) respectively ordered, were successfully synthesized by oxidation of $Sn^{II}_{1.64}(Ta_{1.88}Sn^{IV}_{0.12})O_{6.58}$ pyrochlore. One was a fluorite-related phase, and the other was a rutile-related phase; the rutile-related phase appeared as an impurity in the fluorite-related phase. Those oxidation behaviors of the precursor $Sn^{II}_{1.64}(Ta_{1.88}Sn^{IV}_{0.12})O_{6.58}$ pyrochlore were similar to those of the previous $Sn^{II}_{1.62}(Nb_{1.86}Sn^{IV}_{0.14})O_{6.55}$ pyrochlore. However, the $Sn^{IV}_{0.82}(Ta_{0.94}Sn^{IV}_{0.06})O_{4.11}$ with a cation-ordered α-PbO_2 structure did not appear in the oxidation of the pyrochlore under O_2 atmosphere while the cation-ordered α-PbO_2-related $Sn^{IV}_{0.81}(Nb_{0.93}Sn^{IV}_{0.07})O_{4.085}$ was obtained by the oxidation of $Sn^{II}_{1.62}(Nb_{1.86}Sn^{IV}_{0.14})O_{6.55}$ pyrochlore under O_2 atmosphere. As compared, the XRD profile of the fluorite-related $Sn^{IV}_{0.82}(Ta_{0.94}Sn^{IV}_{0.06})O_{4.11}$ prepared under O_2 atmosphere with that prepared under 1% O_2/Ar atmosphere, e.g., Figs. 5(c) and 6(c), the diffractions of the phase prepared under O_2 atmosphere were distinctly broader than that prepared under 1% O_2/Ar. According to the knowledge for Sn–Nb–O system, it is suggested that the fluorite-related $Sn^{IV}_{0.82}(Ta_{0.94}Sn^{IV}_{0.06})O_{4.11}$ was more unstable under O_2 atmosphere than under 1% O_2/Ar atmosphere. The broader diffractions for the sample oxidized under O_2 atmosphere than those for the sample oxidized under 1% O_2/Ar atmosphere may be originated from the beginning of the transformation from fluorite-related phase into α-PbO_2-related phase. Based on the transformation mechanism and energy barriers of the transformation among the fluorite-, rutile- and α-PbO_2-related phases proposed for Sn–Nb–O system [8], the larger energy barrier from fluorite to α-PbO_2-related phases for Sn–Ta–O system than that for Sn–Nb–O system should explain that α-PbO_2-related phase did not appear in the present Sn–Ta–O system. The more higher oxygen

Table 3
Selected geometric parameters in the present $Sn^{II}_{1.64}(Ta_{1.88}Sn^{IV}_{0.12})O_{6.58}$ pyrochlore and $Sn^{II}_{1.43}(Nb_{1.84}Sn^{IV}_{0.16})O_{6.35}$ pyrochlore reported by Cruz et al.

This study		Reported by Cruz et al.	
Atom	Geometric parameters (nm,°)	Atom	Geometric parameters (nm,°)
Ta–O1^{i} x6	0.197	Nb–O1^{i} x6	0.19813
Sn1–O2	0.222	Sn1–O2	0.2311
Sn1–O2^{viii}	0.240	Sn1–O2^{viii}	0.2317
Sn1–O1^{ii}	0.241	Sn1–O1^{ii}	0.2323
Sn1–O1$^{(iii,iv)}$ x2	0.262	Sn1–O1$^{(iii,iv)}$ x2	0.2536
Sn1–O1$^{(v,vi)}$ x2	0.293	Sn1–O1$^{(v,vi)}$ x2	0.2914
Sn1–O1^{vii}	0.310	Sn1–O1^{vii}	0.3087
Sn2–O2$^{(xv,xvi)}$ x2	0.232	Sn2–O2$^{(xv,xvi)}$ x2	0.2316
Sn2–O1$^{(ix,x)}$ x2	0.245	Sn2–O1$^{(ix,x)}$ x2	0.2375
Sn2–O1$^{(xi,xii)}$ x2	0.278	Sn2–O1$^{(xi,xii)}$ x2	0.2733
Sn2–O1$^{(xiii,viv)}$ x2	0.308	Sn2–O1$^{(xiii,viv)}$ x2	0.3049
O1^{i}–Ta–O1^{xvii}	88.22	O1^{i}–Nb–O1^{xvii}	89.39
O1^{xiii}–Ta–O^{1i}	91.78	O1^{xiii}–Nb–O^{1i}	90.61
O1^{i}–Ta–O1^{xviii}	91.78	O1^{i}–Nb–O1^{xviii}	90.61
O1^{i}–Ta–O1^{xiv}	180.00	O1^{i}–Nb–O1^{xiv}	180.00
O2–Sn1–O2^{viii}	161.6	O2–Sn1–O2^{viii}	160.8
O1^{ii}–Sn1–O1^{iii}	70.54	O1^{ii}–Sn1–O1^{iii}	69.8
O1^{ii}–Sn1–O1^{v}	128.0	O1^{ii}–Sn1–O1^{v}	124.1
O1^{ii}–Sn1–O1^{vii}	172.0	O1^{ii}–Sn1–O1^{vii}	177.7
O1^{iii}–Sn1–O1^{iv}	129.8	O1^{iii}–Sn1–O1^{iv}	132.1
O1^{iii}–Sn1–O1^{v}	65.0	O1^{iii}–Sn1–O1^{v}	61.0
O1^{iii}–Sn1–O1^{vi}	172.0	O1^{iii}–Sn1–O1^{vi}	165.8
O1^{iii}–Sn1–O1^{vii}	117.5	O1^{iii}–Sn1–O1^{vii}	110.7
O1^{v}–Sn1–O1^{vi}	107.6	O1^{v}–Sn1–O1^{vi}	105.4
O1^{v}–Sn1–O1^{vii}	57.3	O1^{v}–Sn1–O1^{vii}	55.3
O2^{xv}–Sn2–O2^{xvi}	163.2	O2^{xv}–Sn2–O2^{xvi}	160.4
O1^{ix}–Sn2–O1^{x}	68.2	O1^{ix}–Sn2–O1^{x}	71.9
O1^{ix}–Sn2–O1^{xi}	124.7	O1^{ix}–Sn2–O1^{xi}	130.2
O1^{ix}–Sn2–O1^{xii}	68.2	O1^{ix}–Sn2–O1^{xii}	65.7
O1^{ix}–Sn2–O1^{xiii}	178.0	O1^{ix}–Sn2–O1^{xiii}	171.3
O1^{ix}–Sn2–O1^{xiv}	124.7	O1^{ix}–Sn2–O1^{xiv}	116.9
O1^{xi}–Sn2–O1^{xii}	167.0	O1^{xi}–Sn2–O1^{xii}	163.4
O1^{xi}–Sn2–O1^{xiii}	107.9	O1^{xi}–Sn2–O1^{xiii}	106.4
O1^{xi}–Sn2–O1^{xiv}	55.8	O1^{xi}–Sn2–O1^{xiv}	57.3
O1^{xiii}–Sn2–O1^{xiv}	55.8	O1^{xiii}–Sn2–O1^{xiv}	54.4

Symmetry codes: (i) y, $1/4-x$, $1/4-z$; (ii) $1/4+y$, $1/4+z$, $1-x$; (iii) x, $1/2+y$, $1/2+z$; (iv) $3/4-z$, x, $3/4-y$; (v) $1/4+y$, $1-x$, $1/4+z$; (vi) $1-x$, $1/4+z$, $1/4+y$; (vii) $3/4-y$, $3/4-z$, x; (viii) $1/4+y$, $1-z$, $1/4+x$; (ix) $-z$, $1/4+y$, $x-3/4$; (x) y, $3/4-x$, $-1/4-z$; (xi) $x-1/2$, y, $z-1/2$; (xii) $1/2-x$, $1/4+z$, $y-1/4$; (xiii) y, $1/4-z$, $1/4-x$; (xiv) $y-1/4$, $x-1/4$, $-z$; (xv) $1/4-z$, x, $1/4-y$; (xvi) $y-1/4$, $1/2-z$, $x-3/4$; (xvii) $-z$, $y-1/4$, $x-1/4$; (xviii) $1/4-x$, $1/4-y$, z.

partial pressure above atmospheric pressure may be required for the appearance of the α-PbO_2-related $Sn^{IV}_{0.82}(Ta_{0.94}Sn^{IV}_{0.06})O_{4.11}$.

The XRD profile of the cation-ordered fluorite-related $Sn^{IV}_{0.82}(Ta_{0.94}Sn^{IV}_{0.06})O_{4.11}$ obtained was distinctly broader than that of the precursor pyrochlore phase; this situation was clearly observed in Fig. 6 as compared

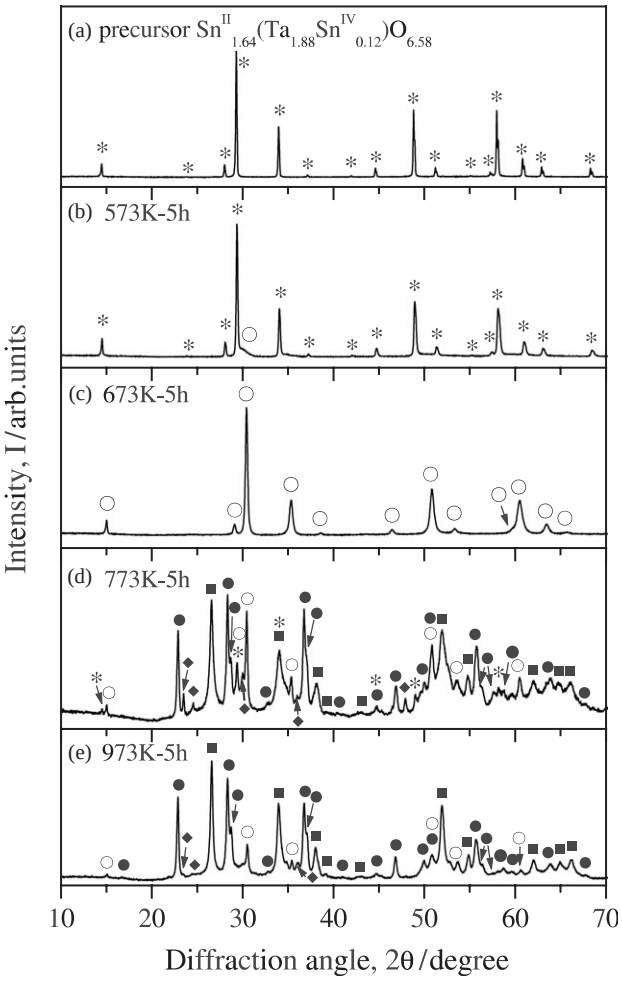

Fig. 5. Powder XRD patterns of the samples obtained by the oxidation of the precursor Sn–Ta–O pyrochlore, $Sn^{II}_{1.64}(Ta_{1.88}Sn^{IV}_{0.12})O_{6.58}$, in O_2 flow. (a) Precursor $Sn^{II}_{1.64}(Ta_{1.88}Sn^{IV}_{0.12})O_{6.58}$ pyrochlore, (b) the precursor oxidized at 573 K, (c) 673 K, (d) 773 K and (e) 973 K. (○) Cation-ordered fluorite-related phase of $Sn^{IV}_{0.82}(Ta_{0.94}Sn^{IV}_{0.06})O_{4.11}$, (■) SnO_2, (●) orthorhombic Ta_2O_5, (♦) monoclinic Ta_2O_5, and (*) pyrochlore-type $Sn^{II}_{1.64}(Ta_{1.88}Sn^{IV}_{0.12})O_{6.58}$.

(c) with (a). The broad diffraction suggested the low crystallinity of the fluorite-related phase. We attempted the structural refinement of the cation-ordered fluorite-related $Sn^{IV}_{0.82}(Ta_{0.94}Sn^{IV}_{0.06})O_{4.11}$ by Rietveld method, but we could not obtain reasonable atomic parameters. Therefore, a speculative discussion of its crystal structure is given here. Taking into consideration the small ionic size of Sn^{IV} and Ta, it is not reasonable that the Sn^{IV} and Ta in the cation-ordered fluorite-related $Sn^{IV}_{0.82}(Ta_{0.94}Sn^{IV}_{0.06})O_{4.11}$ is 8-fold coordination as observed in the ideal fluorite structure. Some of the cations must be 7-fold coordination similar to the case of Sn in $CeSnO_4$ [7]. Seven-fold coordinated cation is a well-known characteristic of the monoclinic ZrO_2 (baddeleyite), and the baddeleyite structure is explained as an intermediate between fluorite structure (8-fold coordination) and rutile or α-PbO_2 structures (6-fold

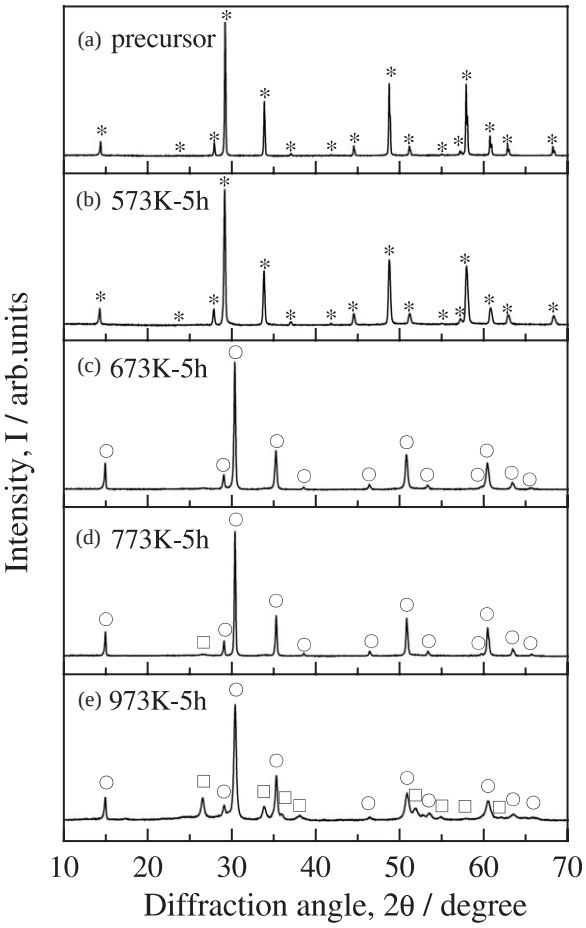

Fig. 6. Powder XRD patterns of the samples obtained by the oxidation of the precursor Sn–Ta–O pyrochlore, $Sn^{II}_{1.64}(Ta_{1.88}Sn^{IV}_{0.12})O_{6.58}$, in 1% O_2/Ar flow. (a) Precursor $Sn^{II}_{1.64}(Ta_{1.88}Sn^{IV}_{0.12})O_{6.58}$ pyrochlore, (b) the precursor oxidized at 573 K, (c) 673 K, (d) 773 K and (e) 973 K. (○) Cation-ordered fluorite-related phase of $Sn^{IV}_{0.82}(Ta_{0.94}Sn^{IV}_{0.06})O_{4.11}$, and (□) Cation-ordered rutile-related $Sn^{IV}_{0.82}(Ta_{0.94}Sn^{IV}_{0.06})O_{4.11}$.

coordination) [13,13–21]. The present cation-ordered fluorite-related $Sn^{IV}_{0.82}(Ta_{0.94}Sn^{IV}_{0.06})O_{4.11}$ should be interpreted as an intermediate between the cation-ordered fluorite as κ-$CeZrO_4$, in which all cations are 8-fold coordinated, and the cation-ordered α-PbO_2 as $Sn^{IV}_{0.81}(Nb^{V}_{0.93}Sn^{IV}_{0.07})O_{4.085}$, in which all cations are 6-fold coordinated. The excess oxygen in $Sn^{IV}_{0.82}(Ta_{0.94}Sn^{IV}_{0.06})O_{4.11}$, 0.11 of oxygen, which were incorporated over the ideal fluorite composition ABO_4, may exist at the similar site as existed in UO_{2+x} [22].

5. Conclusion

We have attempted to synthesize novel metastable phase by oxidation of the precursor pyrochlore phase in Sn–Ta–O system. Two novel metastable $Sn^{IV}_{0.82}(Ta_{0.94}Sn^{IV}_{0.06})O_{4.11}$ were successfully obtained by oxidation of the precursor $Sn^{II}_{1.64}(Ta_{1.88}Sn^{IV}_{0.12})O_{6.58}$ pyrochlore. The one was a fluorite-related phase and the other was a rutile-related phase; the rutile-related phase appeared as an impurity in the fluorite-related phase. Taking into consideration the low oxidation temperature of 673 K, it is not reasonable that the cations in the precursor phase diffuse during the oxidation. Thus, we concluded that respective ordered arrangement of Sn and (0.94Ta + 0.06Sn) in the precursor $Sn^{II}_{1.64}(Ta_{1.88}Sn^{IV}_{0.12})O_{6.58}$ pyrochlore should be left in both the oxidized $Sn^{IV}_{0.82}(Ta_{0.94}Sn^{IV}_{0.06})O_{4.11}$ phases. The cation-ordered α-PbO_2-related $Sn^{IV}_{0.82}(Ta_{0.94}Sn^{IV}_{0.06})O_{4.11}$ could not be obtained in the present conditions, whereas the α-PbO_2-related $Sn^{IV}_{0.81}(Nb_{0.93}Sn^{IV}_{0.07})O_{4.085}$ phase appeared by oxidation of precursor pyrochlore under O_2 atmosphere in Sn–Nb–O system. The energy barrier of the transformation from the fluorite-related phase to α-PbO_2-related phase must be larger in Sn–Ta–O system than in Sn–Nb–O system. Based on this transformation mechanism, the cation-ordered α-PbO_2-related $Sn^{IV}_{0.82}(Ta_{0.94}Sn^{IV}_{0.06})O_{4.11}$ should appear by oxidation of the precursor under the atmosphere with high oxygen partial pressure above atmospheric pressure.

Acknowledgments

This work was supported in part by a Grant-in-Aid for Scientific Research from the Japan Society for the Promotion of Science (Grant No. 15360346) and a Grant-in-Aid from Research Foundation for Materials Science (Tokyo).

References

[1] S. Otsuka-Yao-Matuso, H. Morikawa, N. Izu, K. Okuda, J. Jpn. Inst. Metals 59 (1995) 1237.
[2] S. Otsuka-Yao-Matuso, T. Omata, N. Izu, H. Kishimoto, J. Solid State Chem. 138 (1998) 47.
[3] T. Omata, H. Kishimoto, S. Otsuka-Yao-Matuso, N. Ohtori, N. Umesaki, J. Solid State Chem. 147 (1999) 573.
[4] H. Kishimoto, T. Omata, S. Otsuka-Yao-Matuso, K. Ueda, H. Hosono, H. Kawazoe, J. Alloys Comp. 312 (2000) 94.
[5] J.B. Thomson, A.R. Armstrong, P.G. Bruce, J. Solid State Chem. 148 (1999) 56.
[6] B. Tolla, A. Demourgues, M. Menetrier, L. Fournes, A. Wattiaux, C. R. Acad. Sci. (Paris), Ser. IIc 2 (1999) 139.
[7] B. Tolla, A. Demourgues, O. Isnard, M. Menetrier, M. Pouchard, L. Rabardel, T. Seguelong, J. Mater. Chem. 9 (1999) 3131.
[8] T. Omata, M. Kita, S. Otsuka-Yao-Matuso, M. Katada, J. Alloys Comp. 370 (2004) 80.
[9] T. Omata, M. Kita, S. Otsuka-Yao-Matuso, M. Katada, J. Phys. Chem. Solids 66 (2005) 53.
[10] Y. Syono, S. Akita, Mater. Res. Bull. 3 (1968) 153.
[11] L. Liu, Phys. Chem. Miner. 6 (1980) 187.
[12] J. Haines, J.M. Léger, Phys. Rev. B 48 (1993) 13344.
[13] J. Haines, J.M. Léger, Phys. Rev. B 55 (1997) 11144.
[14] D.J. Stewart, O. Knop, Can. J. Chem. 51 (1973) 1041.
[15] T. Birchall, A.W. Sleight, J. Solid State Chem. 13 (1975) 118.
[16] F. Izumi, T. Ikeda, Mater. Sci. Forum 198 (2000) 321.

[17] L.P. Cruz, J.-M. Savariault, J. Rocha, J.-C. Jumas, J.D. Pedrosa de Jesus, J. Solid State Chem. 156 (2001) 349.
[18] L.P. Cruz, J.-M. Savariault, J. Rocha, Acta Crystallogr. C 57 (2001) 1001.
[19] B.T.M. Willis, Acta Crystallogr. A 34 (1978) 88.
[20] J.K. Dewhurst, J.E. Lowther, Phys. Rev. 57 (1998) 741.
[21] J.E. Lowther, J.K. Dewhurst, Phys. Rev. 60 (1999) 14485.
[22] T. Sasaki, J. Phys.: Condens. Matter 14 (2002) 10557.